

Diffusion of Proteins on Cell Membranes
1D Finite Element Method

Aaron Kaw

Contents

1	Introduction	4
1.1	Abstract	4
1.2	Reading	4
I	Cell and Protein Dynamics	6
2	Structure	7
2.1	Cells	7
2.2	Proteins	8
2.3	Vesicles	8
3	Dynamics	9
3.1	Fusion	9
3.2	Diffusion	10
3.2.1	Delivery Timing	10
3.3	Energetics	10
4	Observations	11
4.1	Electron Micrography	11
4.2	TIRF Microscopy	11
4.2.1	Frame Rate	12
4.2.2	Observation Zone	12
II	Mathematical Model	13
5	Mathematical Background	14
5.1	Goal	14
5.2	Notation	15
5.3	Modelling Theory	16
6	Diffusion	17
6.1	Conservation of Mass	17

6.2	Fick's First Law of Diffusion	17
6.3	Diffusion Equation	18
6.4	Pre-Fusion Parameters	18
6.5	Total Concentration	18
6.6	Fusion	18
6.6.1	Conservation of Surface Area	19
7	Full Fusion	20
7.1	Fusion Parameters	20
7.1.1	Post-Fusion Radii	20
7.1.2	Junction Angle	20
7.1.3	Diffusivity	21
7.2	Initial-and-Boundary Value Problem	21
7.3	Analytical Solution for Constant Diffusivity	21
7.4	Weak Form	23
7.4.1	Parameterisation by Arc Length	24
8	Kiss-and-Run Fusion	25
8.1	Fusion Parameters	25
8.1.1	Post-Fusion Radii	25
8.1.2	Junction Angles	26
8.2	Initial-and-Boundary Value Problem	26
8.3	Weak Form	27
9	Finite Element Method	31
9.1	Conservation of Mathematical Principles	31
9.1.1	Stability and Conservation of Mass	32
9.1.2	32
9.2	Spatial Discretisation	32
9.2.1	Taming Discontinuity	34
9.3	Temporal Discretisation	34
9.4	Mass Matrix	35
9.5	Stiffness Matrix	36
10	TIRF Microscopy Model	38
10.1	TIRF Microscopy Zone	38
10.2	Spot Intensity	38
10.3	Ring Intensity	38
III	Implementation	39
11	Application Programming Interface	40
11.1	Fusion Modes	40
11.2	Diffusion	40
11.3	Intensity	40

11.3.1	Point Spread Function	40
11.3.2	TIRF Zone	40
11.3.3	Spot Intensity	40
11.3.4	Ring Intensity	40
12	Tests	41
12.1	Total Concentration	41
12.2	Junction Flux	41
12.3	Steady State	41
13	Model Usage	42
IV	Mode Discernment	43
14	Total Concentration on Fused Vesicle Membrane	44
15	TIRF Microscopy Simulation	45
16	Regional Intensity	46
16.1	Spot Intensity	46
16.2	Ring Intensity	46
16.3	Point Spread	46
16.4	TIRF Zone	46
16.5	Frame Rate	46
17	Discernment	47
17.1	General Conclusions	47
17.2	Applications	47
17.2.1	Beta Cells	47

Chapter 1

Introduction

1.1 Abstract

Protein delivery to a cell membrane consists of two alternative fusion modes that contrast in energy expenditure and resource-cost. Thus, identifying a cell's bias to either of the two modes can suggest the process acting in the cell. However, current experimental and observational methods for time-dependent fusion events are limited in resolution, obscuring the differences between the two modes. We model both modes, simulate over the parameters spaces of known values for mammalian cells, and compare the theoretical evolution of the fusion and diffusion process. Failure to distinguish the two modes in simulation with infinite resolution can suggest the impossibility in making distinctions with limited resolution. On the other hand, successful distinctions in simulations can suggest the type of observations that may provide further resolution of the process in the laboratory setting.

1.2 Reading

This document is a detailed description of the biological and experimental background, the mathematical model, programmed implementation, and interpretation of results. The audience are graduates and above who have familiarity with the fields of cell biology and the finite element method. Needless to say, the reader can skip to the interpretation at the end of the document.

The first part details the biological background, giving context for the motivation behind developing the diffusion model. The second part provides the mathematical derivation of the model, approximately to a one-to-one relationship with the biological background given. The third part gives a summary of the implementation in the Julia programming language, including the application programming interface (API) from a selection of biological parameters.

The fourth part gives an interpretation of the model results, providing rationale for conclusions.

The topic of this document is effectively divided into [?] ordered stages, found as a structural theme in the contextual, model, implementation, and interpretation descriptions that the reader is encouraged to observe when reading:

1. Fusion
2. Diffusion
3. Observation

Part I

Cell and Protein Dynamics

Chapter 2

Structure

2.1 Cells

Mammalian cells range in volume from 100 to 10'000 micrometers, surrounded by a largely impermeable membrane with a typical thickness of 4 to 10 nanometers [Milo et al., 2010]. The extremely thin nature of the membrane can be demonstrated by scaling the cell size up to that of a watermelon, where the resulting membrane thickness becomes that of a sheet of paper. This membrane is composed of phospholipids, which have hydrophilic heads and hydrophobic tails as shown in Figure TODO.

Phospholipids react to the exposure of water [REF]. When a collection of phospholipids are placed in an aqueous environment, the hydrophobic tails are repelled from the water, whilst the heads are attracted to the water. Typical lipid structures are shown in Figure TODO. These include manifold spheres with tails on the inside and heads on the outside (micelle), or sheet-like structures

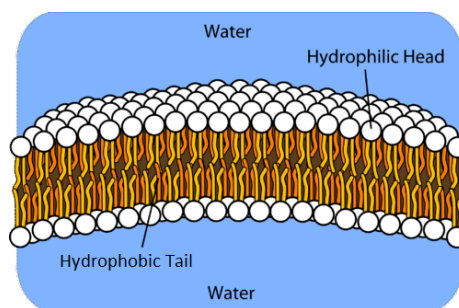


Figure 2.1: Visualisation of the phospholipid structure of cell membranes. Reproduced from [Soult et al., 2020]

referred to as a phospholipid bilayer. These bilayers can form closed objects such as liposomes. Liposomes are generally very small in diameter [REF]. Cellular lipid bilayers are also known as membranes.

2.2 Proteins

The outer cell membrane is largely impermeable. In order to transport molecules such as glucose and proteins in and out of the cell, other protein structures are integrated into the structure of the membrane. Such proteins appear in many forms including peripheral, channel, integral, and internal. These molecules carry out specific functions and are free to move laterally on the membrane. Thus, one may think of these proteins on cell membranes as objects free to move laterally in a viscous fluid [REF].

Some cellular functions the proteins enable include [REF]:

- Transporting materials across the membrane through channels
- Catalysing chemical reactions
- Receiving and sending chemical signals
- Responding to stimuli
- Providing structural support

2.3 Vesicles

Cells have the capacity to change the amount of membrane-embedded proteins on the outer cell membrane via vesicles [REF]. Such vesicles also consist of a phospholipid bilayer structure, and membrane contents such as proteins. Vesicles deliver their contents to different locations inside and outside the cell by merging their membrane with that of the destination. This delivers the fluid contents contained inside the vesicle to the extracellular volume, such as happens in neural signalling, but also, more importantly for the current study, the fusion delivers the membrane-embedded contents to the cell membrane [REF].

Chapter 3

Dynamics

3.1 Fusion

Vesicles are formed by small pieces of membrane budding off larger membrane structures. When vesicles form at the cell membrane to transport material into the cell the process is called endocytosis [REF].

When vesicles deliver material from the cell cytoplasm (internal contents) to the surface, fusing their membranes with the outer cell membrane, the process is called exocytosis [REF]. The process of exocytosis is the motivation and focus of the present study.

When a vesicle needs to deliver its cargo to a membrane, the vesicle is joined or fused with that of the destination. This in general requires energy expenditure by the cell as it is not energetically favourable to expose the lipid tails to the aqueous cellular environment. Cells use protein “grappling hooks” to force the vesicle and destination membranes to join at a circular pore [REF]. These pores are naturally circular, again due to the hydrophobic nature of the lipid tails. After this, one of two things happen, either the vesicle membrane bends to conform to the curvature of the cellular membrane — a process called full fusion or full collapse fusion depicted in Figure TODO — or alternatively the vesicle remains largely intact, and does not fully fuse with the cell membrane. In the latter case, the vesicles retain their shape during the flow of proteins from the vesicle onto the cell, and after a period of time the vesicles detach and return to the cell interior. This process is aptly named kiss-and-run fusion, and is shown in Figure TODO.

3.2 Diffusion

The arrival of membrane proteins at the cell membrane from the fused vesicle results in a local concentration spike. Diffusion of the proteins then redistributes them to equilibrate the concentration across the membrane surfaces [REF]. This diffusion is the central focus of study.

While diffusion in cells can refer to the transport of molecules between the cellular interior and exterior facilitated by proteins [REF], this study uses the term diffusion to refer to the lateral movement of the proteins within the confines of the cellular membrane [REF].

Diffusivity is the measure of the rate of movement of a substance with time in a particular medium. The lateral diffusivity of a membrane is influenced by its composition. Thus diffusivity can vary on the vesicle and cell membranes.

3.2.1 Delivery Timing

Due to TODO, the delivery of membrane proteins via diffusion typically does not start until the vesicle is established in its fusion form.

3.3 Energetics

Vesicular fusion requires energy [REF]. The synthesis of a vesicle also costs resources and energy. Thus, kiss-and-run fusion enables resource and energy saving at the cost of maintaining the small delivery pore at the junction of the two membrane manifolds, which however requires energy. In contrast, full fusion results in the vesicle membrane incorporated into the cell membrane. This costs less energy since the membranes converge to an energetic equilibrium. However, any further protein delivery requires the synthesis of more vesicles [REF].

Chapter 4

Observations

A cell's bias toward either of the two delivery modes may indicate the underlying processes and mechanisms acting in the cell, with regards to energy expenditure and available resources. This is one motivation for tracking vesicular delivery and modality.

4.1 Electron Micrography

Electron micrographs are of slices of frozen cells. This is because the process of obtaining the image is long compared to changes and movements within the cells. Thus, whilst high resolution of the cell such as its surface structure is obtained, there is less information regarding the cellular dynamics.

The processes of both vesicular fusion modes have been observed in electron micrography, as shown in Figure TODO.

4.2 TIRF Microscopy

In Total Internal Reflection Fluorescence (TIRF) Microscopy (TIRFM) proteins are tagged with a fluorescent molecule. The surface to be observed is placed on a microscope coverslip and a laser beam shone on the sample, incident at an angle greater than the critical angle for the coverslip, causing total internal reflection. Not all the energy of the incident light is reflected however, and the evanescent wave, which penetrates the sample, causes the excitation of the fluorophores to depths of around 100 nm, with intensity decaying exponentially. This enables the observation of molecules at the surface of the sample [REF].

In live cell imaging, a sequence of images are recorded, producing a movie of changes occurring at the cell surface [REF].

These frames display pixelated intensity levels at the surface of the cell. An example of such a frame is shown in Figure TODO.

Experimentally, it is often easier to label the membrane embedded contents rather than the contents in the vesicle's interior, allowing experimentalists to also observe these types of fusion events.

The main feature of TIRFM observations of vesicle fusions is the brightness of the spots that appear when the vesicle fuses. An example is shown as the red line plot of the centre profile in Figure TODO. Notice the spike in brightness due to the fusion of the vesicle to the cell, when the vesicle membrane has a high concentration of vesicles relative to the local cell membrane. The subsequent decay in the intensity is due to the diffusion of the proteins from the initial spot region onto the cell membrane [REF].

4.2.1 Frame Rate

Overexposure of the fluoresced proteins results in bleaching [REF]. As a result, TIRFM snapshots are either of high frame rate for a short period of time, or low frame rate over a longer period of time [REF].

4.2.2 Observation Zone

As aforementioned, observable fluorescence decays exponentially with depth from the viewing platform [REF] which provides the advantage of limiting dynamics observations to and around the surface, with the disadvantage of no observation for cellular internals. The latter could however deem depth distinctions difficult.

Also recorded in TIRFM are the approach and departure of vesicles via the gradual appearance of a local spot brightness in the former, and the gradual disappearance in the latter.

Part II

Mathematical Model

Chapter 5

Mathematical Background

5.1 Goal

This study seeks to identify the distinguishing features of the protein dynamics associated with full fusion and kiss-and-run fusion modes. It particularly investigates whether it is theoretically possible to resolve the fusion mode from the evolution of the distribution of proteins at the cell surface.

The movement of proteins on a cell membrane is governed by diffusion. The fusion and diffusion processes are explored for the geometries involved in full fusion and kiss-and-run fusion. The membranes involved are approximated as spherical manifolds.

A classifier for experimental fusion observations is developed here. The main experimental observation is the intensity of the fusion spot, Figure TODO. For the theoretical analogue, the spot intensity is defined to be the normalized total concentration of proteins in the initial spot-region where a vesicle has fused to the cell membrane. The nomenclature is consistent with the fact that the total number of proteins in an area is proportional to the intensity of fluorescence seen in TIRF microscopy.

Due to the limited resolution of the experimental data, it is not possible to observe all the details of the dynamics at a vesicular scale. Instead, experiments track the pixelated spot intensity as a function of discrete time steps. The mathematical models have the advantage of analysis with “infinite” resolution in both space and time.

Of auxiliary usefulness is the intensity of the ring around the fusion spot. Both fusion modes are anticipated to have similar intensity dynamics, yet the surrounding ring is expected to have stronger distinctions. In observations, the ring intensity can distinguish between a transiting vesicle under the surface from an actual fusion event.

Also modelled is the TIRFM observation zone, wherein the fluorescence decays exponentially with depth.

5.2 Notation

The standard Cartesian coordinate system in three dimensions are described using $\vec{x} = (x, y, z)$ with positive directions defined via the right-hand rule. The vertical coordinate z is replaced in some modelling contexts with ξ and ζ , which are simply vertical offsets sharing horizontal coordinates (x, y) .

The dimension of time is represented by the variable t .

Proteins are treated as infinitesimal, parameterised and treated similarly to heat. Symbols of use are u , v and c which will be defined in their respective contexts. The term concentration is used interchangeably with density.

The parameter of the flux of proteins is represented by J as a scalar, or \vec{J} as a vector, and is minimally but vitally explored. It's involvement is implicitly in other parameters.

The rate of diffusion of proteins is termed the diffusivity, notated D .

Distances from the coordinate origin in spherical coordinates is denoted by r as a variable, and R as a constant. The respective polar angle is expressed as φ , ϕ , and ψ introduced as needed with the model derivation.

The use of angle brackets $\langle \bullet \rangle$ are typically used to denote inner products in linear algebra, and integrated averages over time or another continuous parameter in physical sciences. In this paper, a definition similar to both is employed as defined in TODO.

As demonstrated in the previous paragraph, a bullet \bullet is sometimes used as a placeholder for a variable or function.

The same physical parameters are explored in different micro-contexts, required either alternative use of symbol (as above with concentration and vertical coordinate) or symbol embellishment for distinction. for distinction between pre- and post-fusion parameters, a prime \bullet' is used to denote post-fusion parameter. The absence of a prime however does not imply strictly pre-fusion.

The Heaviside function is used extensively in the modelling process, and is denoted $H(x)$, defined as

$$H(x) = \begin{cases} 0 & x < 0 \\ 0.5 & x = 0 \\ 1 & x > 0 \end{cases}$$

δ_{mn} is the Kronecker delta,

$$\delta_{mn} = \begin{cases} 0 & m \neq n \\ 1 & m = n \end{cases}$$

Topological set theory notation is used, particularly $\bar{\bullet}$ to denote set closure, $\partial\bullet$ for the boundary/ies of a set, $\inf \bullet$ and $\sup \bullet$ respectively denoting the infimum and supremum (boundaries) of the set \bullet , and $\text{conv}\bullet$ denoting the convex hull of the set \bullet . Motivation for such uses are for concise expression and this paper does not explore any rigorous topology or differential geometry.

Other set notation used are the classical symbols of \mathbb{R} for the real numbers and \mathbb{Z} for the integers. The strictly positive integers are denoted \mathbb{Z}^+ and to include zero, \mathbb{Z}_0^+ . \mathbb{P} is used to denote the set of valid integer values for an index in the derived models, $\mathbb{P} = \{0, 1, 2, \dots, P-1, P\}$ for $P \in \mathbb{Z}^+$.

5.3 Modelling Theory

The following description is of a model built on the theory of differential equations, the finite element method,

All scenarios analysed in this paper are axisymmetric and restricted to the surface of a sphere.

Metric units are considered consistent, and are not defined until TODO.

Chapter 6

Diffusion

Protein delivery dynamics are here modelled as a scaled concentration diffusion on the surface of static membrane manifolds. Full fusion is modelled on the surface of a sphere, and kiss-and-run fusion on the surface of two truncated, connected spheres. The physical parameters involved in each model are derived from the pre-fusion cell and delivery vesicle parameters. The diffusion equation is then solved on the manifold defined by those parameters.

The membranes are modelled as static due to the diffusion of proteins not starting until the vesicle is established in its fusion form structure, see TODO.

6.1 Conservation of Mass

The diffusion model assumes no source or sink for proteins, hence a conservation of mass expressed as follows.

$$\frac{\partial u}{\partial t} = -\nabla \cdot \vec{J}$$

6.2 Fick's First Law of Diffusion

Fick's first law of diffusion simply states that the flux goes from high to low levels of concentration.

$$\vec{J}(\vec{x}, t) = -D(\vec{x}, t) \nabla u(\vec{x}, t)$$

6.3 Diffusion Equation

The diffusion equation is obtained via equating the flux under the law of mass conservation with Fick's first law of diffusion.

$$\frac{\partial u(\vec{x}, t)}{\partial t} = \nabla \cdot [D(\vec{x}, t) \nabla u(\vec{x}, t)]$$

In spherical coordinates with azimuthal symmetry on the surface of a sphere,

$$r^2 \sin(\varphi) \frac{\partial u}{\partial t} = \frac{\partial}{\partial \varphi} \left(D(\varphi) \sin(\varphi) \frac{\partial u}{\partial \varphi} \right)$$

6.4 Pre-Fusion Parameters

The fusion events in question involve the dynamics of two spherical membranes connecting to form a fused system. Preceding any contact, the physical features of the two membranes are parameterised for their spherical radius and membrane protein diffusivity. Specifically, subscripts \bullet_v and \bullet_c are used to denote parameters for the vesicle and cell respectively. The model input constants are R_v and R_c for the pre-fusion radii and D_v and D_c for the diffusivities.

The fusion events result in geometric deformities that demand the calculation of further post-fusion parameters. However the diffusivities are assumed to persist.

Though it is highly unrealistic for a vesicle to approach the size of the cell, such a scenario provides a convenient way to test the validity of the derived models.

6.5 Total Concentration

The objective output variable of interest is the intensity, otherwise termed the integration of the normalised concentration level over a specified spatial domain Ω .

$$\langle \bullet \rangle_{\Omega} = r^2 \int_{\Omega} \bullet \sin(\varphi) \, d\varphi$$

This definition is later re-derived into a form used due to the model derivation process, given in TODO and TODO.

6.6 Fusion

For both fusion events, the following assumptions are made.

6.6.1 Conservation of Surface Area

Pre-fusion, the vesicle and cell surface areas are given as

$$\begin{aligned} \text{SA}_v &= 4\pi R_v^2 \\ \text{SA}_c &= 4\pi R_c^2 \end{aligned}$$

Chapter 7

Full Fusion

7.1 Fusion Parameters

The process of full fusion results in the vesicle becoming fully incorporated into the geometrical structure of a cell. This results in a post-fusion sphere, which is modelled with polar angle $\varphi \in \bar{\Omega}$ with $\Omega = (0, \pi)$. The vesicle becomes fused as a polar cap on the fused system. The system maintains its axisymmetry.

7.1.1 Post-Fusion Radii

Under the assumption of surface area preservation,

$$\begin{aligned} \text{SA}_{\text{full fusion}} &= \text{SA}_v + \text{SA}_c \\ \Rightarrow 4\pi R'^2 &= 4\pi R_v^2 + 4\pi R_c^2 \\ \Rightarrow R' &= \sqrt{R_v^2 + R_c^2} \end{aligned}$$

where the post-fusion spherical radius is denoted as $R' > 0$.

7.1.2 Junction Angle

The fused system results in the vesicle and cell membrane meeting at a location termed the junction, denoted by the polar angle as φ_j . The location of this junction is derived from the fact that the vesicle's preserved surface area occupies

the fused sphere as a spherical cap.

$$\begin{aligned}
\text{SA}_{\text{cap}} &= \text{SA}_v \\
\Rightarrow 2\pi R'^2(1 - \cos(\varphi_j)) &= 4\pi R_v^2 \\
\Rightarrow \varphi_j &= \cos^{-1}\left(1 - \frac{2R_v^2}{R'^2}\right) \\
&= \cos^{-1}\left(\frac{R_c^2 - R_v^2}{R'^2}\right)
\end{aligned}$$

for $\varphi_j \in \Omega$.

7.1.3 Diffusivity

The full fusion model assumes conservation of diffusivity, resulting in a junction consisting of a potential diffusivity transition. This is modelled as Heaviside.

$$D(\varphi) = D_v H(\varphi_j - \varphi) + D_c H(\varphi - \varphi_j)$$

7.2 Initial-and-Boundary Value Problem

The diffusion equation applied to the full fusion model with parameters defined above provides the initial-and-boundary value problem as follows.

$$\begin{aligned}
R'^2 \sin(\varphi) \frac{\partial u(\varphi, t)}{\partial t} &= \frac{\partial}{\partial \varphi} \left(D(\varphi) \sin(\varphi) \frac{\partial u(\varphi, t)}{\partial \varphi} \right) & \varphi \in \Omega & \quad t > 0 \\
u(\varphi, t) &= H(\varphi_j - \varphi) & \varphi \in \overline{\Omega} & \quad t = 0 \\
\frac{\partial u(\varphi, t)}{\partial \varphi} &= 0 & \varphi \in \partial\Omega & \quad t \geq 0
\end{aligned}$$

7.3 Analytical Solution for Constant Diffusivity

The frontier of analytical solution methods for the diffusion problem specified above involves constant diffusivity. Though deriving such a solution is of limited scope, it provides a useful validity test for the implementation.

By constant diffusivity, $D(\varphi) = D$ so

$$\frac{R'^2}{D} \frac{\partial u(\varphi, t)}{\partial t} = \frac{1}{\sin(\varphi)} \frac{\partial}{\partial \varphi} \left(\sin(\varphi) \frac{\partial u(\varphi, t)}{\partial \varphi} \right)$$

Via the method of separation of variables for partial differential equations, we assume

$$u(\varphi, t) = \Phi(\phi)T(t)$$

and substitution into the full fusion diffusion equation yields the pair of equations

$$\begin{aligned} 0 &= \frac{dT(t)}{dt} + \frac{\lambda D}{R'^2} T(t) \\ 0 &= \frac{1}{\sin(\varphi)} \frac{d}{d\varphi} \left(\sin(\varphi) \frac{d\Phi(\varphi)}{d\varphi} \right) + \lambda \Phi(\varphi) \end{aligned}$$

with separation constant $-\lambda$. The temporal equation admits solution form

$$T(t) = \exp \left\{ \frac{-\lambda D}{R'^2} t \right\}$$

Let our spatial transform project to the vertical coordinate $z = \cos(\varphi)$ with $\Phi(\varphi) = Z(z)$, so

$$0 = \frac{d}{dz} \left((1 - z^2) \frac{dZ(z)}{dz} \right) + \lambda Z(z)$$

which admits eigenfunction solutions of the form

$$Z_n(z) = P_n(z) \quad n = 0, 1, 2, \dots$$

where P_n is the n^{th} Legendre Polynomial of the first kind, with eigenvalues

$$\lambda_n = n(n+1) \quad n = 0, 1, 2, \dots$$

and our solution holds the form

$$u(\varphi, t) = \sum_{n=0}^{\infty} c_n P_n(\cos(\varphi)) \exp \left\{ \frac{-\lambda_n D}{R'^2} t \right\}$$

Applying the initial condition (with vertical coordinate for clarity)¹,

$$\begin{aligned} H(z - z_j) &= \sum_{n=0}^{\infty} c_n P_n(z) \\ \Rightarrow H(z - z_j) P_m(z) &= P_m(z) \sum_{n=0}^{\infty} c_n P_n(z) \quad m = 0, 1, 2, \dots \\ &= \sum_{n=0}^{\infty} c_n P_m(z) P_n(z) \quad m = 0, 1, 2, \dots \\ \Rightarrow \int_{-1}^1 H(z - z_j) P_m(z) dz &= \int_{-1}^1 \sum_{n=0}^{\infty} c_n P_m(z) P_n(z) dz \quad m = 0, 1, 2, \dots \\ &= \sum_{n=0}^{\infty} c_n \int_{-1}^1 P_m(z) P_n(z) dz \quad m = 0, 1, 2, \dots \\ &= \sum_{n=0}^{\infty} c_n \frac{2\delta_{mn}}{2n+1} \end{aligned}$$

¹ Author Note: Check validity of interchanging infinite sum with definite integral.

and for $m = 0$,

$$\begin{aligned}\text{LHS} &= \int_{z_j}^1 dz \\ &= 1 - z_j\end{aligned}$$

but for $m = 1, 2, 3, \dots$,²

$$\begin{aligned}\text{LHS} &= \int_{-1}^1 H(z - z_j) P_m(z) dz \\ &= \int_{z_j}^1 P_m(z) dz \\ &= \frac{1}{2m+1} [P_{m+1}(z) - P_{m-1}(z)]_{z_j}^1 \\ &= \frac{P_{m+1}(z_j) - P_{m-1}(z_j)}{2m+1}\end{aligned}$$

thus for $m = n$,

$$c_n = \begin{cases} \frac{1 - \cos(\phi_j)}{2} & n = 0 \\ \frac{P_{n+1}(\cos \phi_j) - P_{n-1}(\cos \phi_j)}{2} & n = 1, 2, 3, \dots \end{cases}$$

7.4 Weak Form

The numerical solution in prospect requires reformulation of the differential equation in weak form as follows. With $w(\varphi)$ the test function,

$$\begin{aligned}R'^2 \sin(\varphi) \frac{\partial u(\varphi, t)}{\partial t} &= \frac{\partial}{\partial \varphi} \left(D(\varphi) \sin(\varphi) \frac{\partial u(\varphi, t)}{\partial \varphi} \right) \\ R'^2 \sin(\varphi) \frac{\partial u(\varphi, t)}{\partial t} w(\varphi) &= \frac{\partial}{\partial \varphi} \left(D(\varphi) \sin(\varphi) \frac{\partial u(\varphi, t)}{\partial \varphi} \right) w(\varphi) \\ R'^2 \int_{\Omega} \sin(\varphi) \frac{\partial u(\varphi, t)}{\partial t} w(\varphi) d\varphi &= \int_{\Omega} \frac{\partial}{\partial \varphi} \left(D(\varphi) \sin(\varphi) \frac{\partial u(\varphi, t)}{\partial \varphi} \right) w(\varphi) d\varphi \\ \left\langle \frac{\partial u(\varphi, t)}{\partial t} w(\varphi) \right\rangle &= \left[D(\varphi) \sin(\varphi) \frac{\partial u(\varphi, t)}{\partial \varphi} w(\varphi) \right]_{\Omega} - \int_{\Omega} D(\varphi) \sin(\varphi) \frac{\partial u(\varphi, t)}{\partial \varphi} \frac{dw(\varphi)}{d\varphi} d\varphi \\ \left\langle \frac{\partial u(\varphi, t)}{\partial t} w(\varphi) \right\rangle &= - \int_{\Omega} D(\varphi) \sin(\varphi) \frac{\partial u(\varphi, t)}{\partial \varphi} \frac{dw(\varphi)}{d\varphi} d\varphi \\ \left\langle \frac{\partial u(\varphi, t)}{\partial t} w(\varphi) \right\rangle &= - \frac{1}{2\pi R'^2} \left\langle D(\varphi) \frac{\partial u(\varphi, t)}{\partial \varphi} \frac{dw(\varphi)}{d\varphi} \right\rangle\end{aligned}$$

²Author note: reference identity

yielding the weak form

$$0 = \left\langle \frac{\partial u(\varphi, t)}{\partial t} w(\varphi) \right\rangle + \frac{1}{R'^2} \left\langle D(\varphi) \frac{\partial u(\varphi, t)}{\partial \varphi} \frac{dw(\varphi)}{d\varphi} \right\rangle$$

with total concentration

$$\langle \bullet \rangle = R'^2 \int_{\Omega} \sin(\varphi) \bullet \, d\varphi$$

7.4.1 Parameterisation by Arc Length

By foresight of the kiss-and-run fusion modelling, we parameterize the full fusion weak form by arc length.

$$\varphi = \frac{s(\varphi)}{R'}$$

providing the new weak form

$$0 = \left\langle \frac{\partial u(\varphi, t)}{\partial t} w(\varphi) \right\rangle + \left\langle D(\varphi) \frac{\partial u(\varphi, t)}{\partial \varphi} \frac{dw(\varphi)}{d\varphi} \right\rangle$$

with

$$\begin{aligned} \omega(s) &= \frac{s}{R'} \\ \langle \bullet \rangle &= 2\pi R' \int_{\Gamma} \sin(\omega(s)) \bullet \, ds \end{aligned}$$

Chapter 8

Kiss-and-Run Fusion

8.1 Fusion Parameters

The process of kiss-and-run fusion results in the vesicle mostly retaining its spherical shape. The cell similarly retains its shape, but both membranes attain an opening or pore of circular geometry with radius denoted R_j . The fused system is assigned two coordinate systems, one for each membrane with polar angles $\phi \in \Omega_v$ for the vesicle and $\psi \in \Omega_c$ on the cell. The respective domains are derived as following, such that $|\Omega_v| = \phi_v$ and $|\Omega_c| = \psi_c$.

8.1.1 Post-Fusion Radii

Under the assumption of surface area preservation, the vesicle undergoes perforation resulting in a polar cap domain void.

$$\begin{aligned} \text{SA}'_v &= \text{SA}_v \\ \Rightarrow 2\pi R_v'^2 \int_0^{\phi_v} \sin \phi \, d\phi &= 4\pi R_v^2 \\ \Rightarrow R_v'^2 (1 - \cos \phi_v) &= 2R_v^2 \end{aligned}$$

Also note from the trigonometry,

$$\cos(\phi_v) = \frac{-\sqrt{R_v'^2 - R_j^2}}{R_v'}$$

where the negative root arises from our choice of ϕ_v in the second quadrant. Thus,

$$\begin{aligned}
R_v'^2(1 - \cos \phi_v) &= 2R_v^2 \\
\Rightarrow R_v'^2 \left(1 + \frac{\sqrt{R_v'^2 - R_j^2}}{R_v'} \right) &= 2R_v^2 \\
\Rightarrow R_v'^2 + R_v' \sqrt{R_v'^2 - R_j^2} &= 2R_v^2 \\
\Rightarrow \sqrt{R_v'^2 - R_j^2} &= \frac{2R_v^2 - R_v'^2}{R_v'} \\
\Rightarrow R_v'^2 - R_j^2 &= \frac{(2R_v^2 - R_v'^2)^2}{R_v'^2} \\
\Rightarrow R_v'^4 - R_j^2 R_v'^2 &= 4R_v^4 - 4R_v^2 R_v'^2 + R_v'^4 \\
\Rightarrow -R_j^2 R_v'^2 &= 4R_v^4 - 4R_v^2 R_v'^2 \\
\Rightarrow R_v'^2 (4R_v^2 - R_j^2) &= 4R_v^4 \\
\Rightarrow R_v'^2 &= \frac{4R_v^4}{4R_v^2 - R_j^2} \\
\Rightarrow R_v' &= \frac{2R_v^2}{\sqrt{4R_v^2 - R_j^2}}
\end{aligned}$$

By the same reasoning,

$$R_c' = \frac{2R_c^2}{\sqrt{4R_c^2 - R_j^2}}$$

8.1.2 Junction Angles

By the geometry,

$$\begin{aligned}
\phi_v &= \pi - \sin^{-1} \left(\frac{R_j}{R_v'} \right) \\
\psi_c &= \pi - \sin^{-1} \left(\frac{R_j}{R_c'} \right)
\end{aligned}$$

8.2 Initial-and-Boundary Value Problem

The domain of our differential equation is of two connected truncated spheres, connected at their truncations.

$$\begin{aligned}
\Omega_v &= (0, \phi_v) \\
\Omega_c &= (\pi - \psi_c, \pi)
\end{aligned}$$

The initial-and-boundary value problem is of a connection of two systems such that

$$\begin{aligned} R_v'^2 \sin(\phi) \frac{\partial v(\phi, t)}{\partial t} &= D_v \frac{\partial}{\partial \phi} \left(\sin(\phi) \frac{\partial v(\phi, t)}{\partial \phi} \right) & \phi \in \Omega_v & \quad t \geq 0 \\ R_c'^2 \sin(\psi) \frac{\partial c(\psi, t)}{\partial t} &= D_c \frac{\partial}{\partial \psi} \left(\sin(\psi) \frac{\partial c(\psi, t)}{\partial \psi} \right) & \psi \in \Omega_c & \quad t \geq 0 \end{aligned}$$

Initially,

$$\begin{aligned} v(\phi, t) &= 1 & \phi \in \Omega_v & \quad t = 0 \\ c(\psi, t) &= 0 & \psi \in \Omega_c & \quad t = 0 \end{aligned}$$

At the junction,

$$\begin{aligned} v(\phi, t) &= c(\psi, t) & \phi = \sup \Omega_v & \quad \psi = \inf \Omega_c & \quad t \geq 0 \\ \frac{D_v}{R_v'} \frac{\partial v(\phi, t)}{\partial \phi} &= \frac{D_c}{R_c'} \frac{\partial c(\psi, t)}{\partial \psi} & \phi = \sup \Omega_v & \quad \psi = \inf \Omega_c & \quad t \geq 0 \end{aligned}$$

And initially at the junction,

$$v(\phi, t) = c(\psi, t) = 0.5 \quad \phi \in \Omega_v \quad \psi \in \Omega_c \quad t \in \mathbb{R}_0^+$$

imitating a Heaviside transition.

8.3 Weak Form

The weak form is developed with $f(\phi)$ and $g(\psi)$ as test functions.

On the vesicle,

$$\begin{aligned} R_v'^2 \sin(\phi) \frac{\partial v(\phi, t)}{\partial t} &= D_v \frac{\partial}{\partial \phi} \left(\sin(\phi) \frac{\partial v(\phi, t)}{\partial \phi} \right) \\ R_v'^2 \sin(\phi) \frac{\partial v(\phi, t)}{\partial t} f(\phi) &= D_v \frac{\partial}{\partial \phi} \left(\sin(\phi) \frac{\partial v(\phi, t)}{\partial \phi} \right) f(\phi) \\ R_v'^2 \int_{\Omega_v} \sin(\phi) \frac{\partial v(\phi, t)}{\partial t} f(\phi) \, d\phi &= D_v \int_{\Omega_v} \frac{\partial}{\partial \phi} \left(\sin(\phi) \frac{\partial v(\phi, t)}{\partial \phi} \right) f(\phi) \, d\phi \\ R_v'^2 \int_{\Omega_v} \sin(\phi) \frac{\partial v(\phi, t)}{\partial t} f(\phi) \, d\phi &= D_v \int_{\Omega_v} \frac{\partial}{\partial \phi} \left(\sin(\phi) \frac{\partial v(\phi, t)}{\partial \phi} \right) f(\phi) \, d\phi \\ \left\langle \frac{\partial v(\phi, t)}{\partial t} f(\phi) \right\rangle_v &= D_v \left(\left[\sin(\phi) \frac{\partial v(\phi, t)}{\partial \phi} f(\phi) \right]_{\Omega_v} - \int_{\Omega_v} \sin(\phi) \frac{\partial v(\phi, t)}{\partial \phi} \frac{\partial f(\phi)}{\partial \phi} \, d\phi \right) \\ \left\langle \frac{\partial v(\phi, t)}{\partial t} f(\phi) \right\rangle_v &= D_v \left(\left[\sin(\phi_v) \frac{\partial v(\phi_v, t)}{\partial \phi} f(\phi_v) - 0 \right] - \frac{1}{2\pi R_v'^2} \left\langle \frac{\partial v(\phi, t)}{\partial \phi} \frac{\partial f(\phi)}{\partial \phi} \right\rangle \right) \\ \left\langle \frac{\partial v(\phi, t)}{\partial t} f(\phi) \right\rangle_v &= D_v \left(\sin(\phi_v) \frac{\partial v(\phi_v, t)}{\partial \phi} f(\phi_v) - \frac{1}{2\pi R_v'^2} \left\langle \frac{\partial v(\phi, t)}{\partial \phi} \frac{\partial f(\phi)}{\partial \phi} \right\rangle \right) \end{aligned}$$

On the cell,

$$\begin{aligned}
R_c'^2 \sin(\psi) \frac{\partial c(\psi, t)}{\partial t} &= D_c \frac{\partial}{\partial \psi} \left(\sin(\psi) \frac{\partial c(\psi, t)}{\partial \psi} \right) \\
\left\langle \frac{\partial c(\psi, t)}{\partial t} g(\psi) \right\rangle_c &= D_c \left(\left[\sin(\psi) \frac{\partial c(\psi, t)}{\partial \psi} g(\psi) \right]_{\Omega_v} - \int_{\Omega_v} \sin(\psi) \frac{\partial c(\psi, t)}{\partial \psi} \frac{\partial g(\psi)}{\partial \psi} d\psi \right) \\
\left\langle \frac{\partial c(\psi, t)}{\partial t} g(\psi) \right\rangle_c &= D_c \left(\left[0 - \sin(\pi - \psi_v) \frac{\partial c(\pi - \psi_v, t)}{\partial \psi} g(\pi - \psi_v) \right] - \frac{1}{2\pi R_c'^2} \left\langle \frac{\partial c(\psi, t)}{\partial \psi} \frac{\partial g(\psi)}{\partial \psi} \right\rangle \right) \\
\left\langle \frac{\partial c(\psi, t)}{\partial t} g(\psi) \right\rangle_c &= -D_c \left(\sin(\pi - \psi_v) \frac{\partial c(\pi - \psi_v, t)}{\partial \psi} g(\pi - \psi_v) + \frac{1}{2\pi R_c'^2} \left\langle \frac{\partial c(\psi, t)}{\partial \psi} \frac{\partial g(\psi)}{\partial \psi} \right\rangle \right)
\end{aligned}$$

Adding the two expressions,

$$\begin{aligned}
&\left\langle \frac{\partial v(\phi, t)}{\partial t} f(\phi) \right\rangle_v + \left\langle \frac{\partial c(\psi, t)}{\partial t} g(\psi) \right\rangle_c \\
&= D_v \sin(\phi_v) \frac{\partial v(\phi_v, t)}{\partial \phi} f(\phi_v) - D_c \sin(\pi - \psi_v) \frac{\partial c(\pi - \psi_v, t)}{\partial \psi} g(\pi - \psi_v) \\
&\quad - \left(\frac{D_v}{R_v'^2} \left\langle \frac{\partial v(\phi, t)}{\partial \phi} \frac{\partial f(\phi)}{\partial \phi} \right\rangle + \frac{D_c}{R_c'^2} \left\langle \frac{\partial c(\psi, t)}{\partial \psi} \frac{\partial g(\psi)}{\partial \psi} \right\rangle \right)
\end{aligned}$$

then substituting the membrane angle sizes

$$\begin{aligned}
&\left(\left\langle \frac{\partial v(\phi, t)}{\partial t} f(\phi) \right\rangle_v + \left\langle \frac{\partial c(\psi, t)}{\partial t} g(\psi) \right\rangle_c \right) \\
&= D_v \frac{R_j}{R_v'} \frac{\partial v(\phi_v, t)}{\partial \phi} f(\phi_v) - D_c \frac{R_j}{R_c'} \frac{\partial c(\pi - \psi_v, t)}{\partial \psi} g(\pi - \psi_v) \\
&\quad - \left(\frac{D_v}{R_v'^2} \left\langle \frac{\partial v(\phi, t)}{\partial \phi} \frac{\partial f(\phi)}{\partial \phi} \right\rangle + \frac{D_c}{R_c'^2} \left\langle \frac{\partial c(\psi, t)}{\partial \psi} \frac{\partial g(\psi)}{\partial \psi} \right\rangle \right)
\end{aligned}$$

Select $f(\phi)$ and $g(\psi)$ such that

$$f(\phi_v) = g(\pi - \psi_v).$$

so

$$\begin{aligned}
0 &= \left\langle \frac{\partial v(\phi, t)}{\partial t} f(\phi) \right\rangle_v + \left\langle \frac{\partial c(\psi, t)}{\partial t} g(\psi) \right\rangle_c \\
&\quad + \frac{D_v}{R_v'^2} \left\langle \frac{\partial v(\phi, t)}{\partial \phi} \frac{\partial f(\phi)}{\partial \phi} \right\rangle + \frac{D_c}{R_c'^2} \left\langle \frac{\partial c(\psi, t)}{\partial \psi} \frac{\partial g(\psi)}{\partial \psi} \right\rangle
\end{aligned}$$

Define arc-length transformation such that

$$\begin{aligned}
s_j &= R_v' \phi_v \\
s_P &= s_j + R_c' \psi_c \\
s &= \begin{cases} R_v' \phi & \phi \in \Omega_v \\ s_j + R_c'(\psi + \psi_c - \pi) & \psi \in \Omega_c \end{cases}
\end{aligned}$$

so inverse transformations are

$$\begin{aligned}
\Gamma_v &= (0, s_j) \\
\Gamma_c &= (s_j, s_P) \\
\Gamma &= \text{conv}(\Gamma_v \cup \Gamma_c) \\
\phi(s) &= \frac{s}{R'_v} \\
\psi(s) &= \frac{s - s_j}{R'_c} + \pi - \psi_c \\
\omega(s) &= \begin{cases} \phi(s) & s \in \Gamma_v \\ \psi(s) & s \in \Gamma_c \end{cases}
\end{aligned}$$

and define $u(s, t)$ such that

$$u(s, t) = \begin{cases} v(\phi(s), t) & s \in \Gamma_v \\ c(\psi(s), t) & s \in \Gamma_c \end{cases}$$

so derivatives become

$$\begin{aligned}
d\phi &= \frac{1}{R'_v} ds \\
d\psi &= \frac{1}{R'_c} ds \\
\frac{\partial v(\phi, t)}{\partial \phi} &= R'_v \frac{\partial u(s, t)}{\partial s} \\
\frac{\partial c(\psi, t)}{\partial \psi} &= R'_c \frac{\partial u(s, t)}{\partial s}
\end{aligned}$$

and define

$$w(s) = \begin{cases} f(\phi(s), t) & s \in \Gamma_v \\ g(\psi(s), t) & s \in \Gamma_c \end{cases}$$

so our weak form becomes

$$\begin{aligned}
0 &= \left\langle \frac{\partial v(\phi, t)}{\partial t} f(\phi) \right\rangle_v + \left\langle \frac{\partial c(\psi, t)}{\partial t} g(\psi) \right\rangle_c \\
&\quad + \frac{D_v}{R_v'^2} \left\langle \frac{\partial v(\phi, t)}{\partial \phi} \frac{\partial f(\phi)}{\partial \phi} \right\rangle + \frac{D_c}{R_c'^2} \left\langle \frac{\partial c(\psi, t)}{\partial \psi} \frac{\partial g(\psi)}{\partial \psi} \right\rangle \\
0 &= R_v'^2 \int_{\Omega_v} \sin(\phi) \frac{\partial v(\phi, t)}{\partial t} f(\phi) d\phi + R_c'^2 \int_{\Omega_c} \sin(\psi) \frac{\partial c(\psi, t)}{\partial t} g(\psi) d\psi \\
&\quad + D_v \int_{\Omega_v} \sin(\phi) \frac{\partial v(\phi, t)}{\partial \phi} \frac{\partial f(\phi)}{\partial \phi} d\phi + D_c \int_{\Omega_c} \sin(\psi) \frac{\partial c(\psi, t)}{\partial \psi} \frac{\partial g(\psi)}{\partial \psi} d\psi \\
0 &= R_v' \int_{\Gamma_v} \sin(\phi(s)) \frac{\partial u(s, t)}{\partial t} w(s) ds + R_c' \int_{\Gamma_c} \sin(\psi(s)) \frac{\partial u(s, t)}{\partial t} w(s) ds \\
&\quad + D_v \int_{\Gamma_v} \sin(\phi(s)) \frac{\partial u(s, t)}{\partial s} \frac{dw(s)}{ds} ds + D_c \int_{\Gamma_c} \sin(\psi(s)) \frac{\partial u(s, t)}{\partial s} \frac{dw(s)}{ds} ds \\
0 &= \int_{\Gamma} \sin(\omega(s)) R'(s) \frac{\partial u(s, t)}{\partial t} w(s) + \int_{\Gamma} \sin(\omega(s)) D(s) \frac{\partial u(s, t)}{\partial s} \frac{dw(s)}{ds} ds
\end{aligned}$$

yielding our weak form in arc-length

$$0 = \left\langle \frac{\partial u(s, t)}{\partial t} w(s) \right\rangle + \left\langle \frac{D(s)}{R'(s)} \frac{\partial u(s, t)}{\partial s} \frac{dw(s)}{ds} \right\rangle$$

with

$$\begin{aligned}
R'(s) &= \begin{cases} R_v' & s \in \Gamma_v \\ R_c' & s \in \Gamma_c \end{cases} \\
\langle \bullet \rangle &= \int R'(s) \sin(\omega(s)) \bullet ds
\end{aligned}$$

Chapter 9

Finite Element Method

The rigour of approximating the weak form's solution via projection onto a space of square-integrable piecewise-linear functions is not explicitly explored here. However, the theory that follows is taken from such. It will be stated however that the definition of the angle bracket operator operating on a function \bullet is inspired from the inner product defined on the function space operating on \bullet with one. That is,

$$\langle \bullet \rangle = \langle \bullet, 1 \rangle$$

The finite element method expressed generically for the fusion modes of full and kiss-and-run takes a weak formulation

$$0 = \left\langle \frac{\partial u(s, t)}{\partial t} w(s) \right\rangle + \left\langle \frac{D(s)}{R(s)} \frac{\partial u(s, t)}{\partial s} \frac{dw(s)}{ds} \right\rangle$$

with

$$\langle \bullet \rangle = \int_{\Gamma} R(s) \sin(\omega(s)) \bullet ds$$

for Γ , s , $D(s)$, $R(s)$, and $\omega(s)$ defined by the fusion mode model.

9.1 Conservation of Mathematical Principles

By the involvedness of the derivation and for the testing of implementation, the developed model is investigated for validity through application of the first principles it is derived from.

9.1.1 Stability and Conservation of Mass

The finite element method is unconditionally stable for this problem. To see this, note that the weak form given above is valid for arbitrary w . Choosing $w = 1$,

$$0 = \left\langle \frac{\partial u(s, t)}{\partial t} \right\rangle = \frac{\partial}{\partial t} \langle u(s, t) \rangle$$

which is also a statement of conservation. This is to say, the total concentration of proteins is preserved for all time.

In function space theory, this relationship would be expressed with the \mathcal{L}^1 norm.

9.1.2

Another essential feature of the model must be that TODO.

To see this, let $w = u(s, t)$ be time-dependent. Note that in the algebra and calculus manipulations in the derivations, the test functions were never subjected to the time derivative¹.

$$\begin{aligned} 0 &= \left\langle u(s) \frac{\partial u(s, t)}{\partial t} \right\rangle + \left\langle \frac{D(s)}{R(s)} \left(\frac{\partial u(s, t)}{\partial s} \right)^2 \right\rangle \\ &= \left\langle \frac{1}{2} \frac{\partial}{\partial t} (u^2(s, t)) \right\rangle + \left\langle \frac{D(s)}{R(s)} \left(\frac{\partial u(s, t)}{\partial s} \right)^2 \right\rangle \\ &= \frac{1}{2} \frac{\partial}{\partial t} \langle u^2(s, t) \rangle + \left\langle \frac{D(s)}{R(s)} \left(\frac{\partial u(s, t)}{\partial s} \right)^2 \right\rangle \\ &\Rightarrow \frac{\partial}{\partial t} \langle u^2(s, t) \rangle = -2 \left\langle \frac{D(s)}{R(s)} \left(\frac{\partial u(s, t)}{\partial s} \right)^2 \right\rangle \end{aligned}$$

where the $\langle \bullet \rangle$ on the RHS is always positive, thus any change of concentration level over time is TODO.

In function space theory, this relationship would be expressed with the \mathcal{L}^2 norm.

9.2 Spatial Discretisation

Select positive integers p_j and P such that

$$p_j < P$$

Define

$$\mathbb{P} = \{0, 1, 2, \dots, P\}$$

¹Author note: check!

Select values s_p for $p \in \mathbb{P}$ such that

$$0 = s_0 < s_1 < \cdots < s_{p_j-1} < s_{p_j} = s_j < s_{p_j+1} < \cdots < s_{P-1} < s_P$$

Define their spacing,

$$h_p = s_p - s_{p-1} \quad s \in \mathbb{P}^+$$

Define hat functions such that

$$\Lambda_p(s) = \begin{cases} 1 & s = s_p \\ \frac{s - s_{p-1}}{h_p} & s \in (s_{p-1}, s_p) \\ \frac{s_{p+1} - s}{h_{p+1}} & s \in (s_p, s_{p+1}) \\ 0 & \text{otherwise} \end{cases}$$

Transform the weak form into a system of equations by selecting

$$w(s) = \Lambda_p(s) \quad p \in \mathbb{P}$$

so

$$0 = \left\langle \frac{\partial u(s, t)}{\partial t} \Lambda_p(s) \right\rangle + \left\langle \frac{D(s)}{R(s)} \frac{\partial u(s, t)}{\partial s} \frac{\partial \Lambda_p(s)}{\partial s} \right\rangle \quad p \in \mathbb{P}$$

Project the solution $u(s, t)$ onto the space of piecewise-linear functions defined on the discrete grid s_p , and define this projection as

$$u_h(s, t) = \sum_{q=0}^P U_q(t) \Lambda_q(s)$$

and impose this by substitution so

$$0 = \frac{\partial U_q(t)}{\partial t} \langle \Lambda_q(s) \Lambda_p(s) \rangle + U_q(t) \left\langle \frac{D(s)}{R(s)} \frac{\partial \Lambda_q(s)}{\partial s} \frac{\partial \Lambda_p(s)}{\partial s} \right\rangle$$

in Einstein notation for clarity.

Define

$$\begin{aligned} \vec{U}(t) &= [U_0(t) \ U_1(t) \ \cdots \ U_P(t)]^T \\ [M]_{pq} &= \langle \Lambda_q(s) \Lambda_p(s) \rangle \\ [S]_{pq} &= \left\langle \frac{D(s)}{R(s)} \frac{\partial \Lambda_q(s)}{\partial s} \frac{\partial \Lambda_p(s)}{\partial s} \right\rangle \end{aligned}$$

so we have our system

$$0 = M \frac{d\vec{U}(t)}{dt} + S \vec{U}(t)$$

with mass matrix M and stiffness matrix S .

9.2.1 Taming Discontinuity

A Heaviside transition of parameter values is located at the junction in both fusion modes. An optimal selection of spatial grid spacing minimizes the possibility of violating the law of conservation. This motivates placing a large concentration of points around the junction point. The junction itself must also be a grid point.

We apply cubic spacing on the vesicle and cell domains separately.

The vesicular gridding must satisfy

$$s_0 = 0s_{p_j} = s_j$$

and be concave down, which leads to

$$s_p = s_j \left(1 - \left(1 - \frac{p}{p_j} \right)^3 \right)$$

The cellular gridding similarly must satisfy

$$\begin{aligned} s_{p_j} &= s_j \\ s_P &= s_P \end{aligned}$$

and must be concave up, leading to

$$s_p = s_j + (s_P - s_j) \left(\frac{p - p_j}{P - p_j} \right)^3$$

9.3 Temporal Discretisation

Due to stiffness, we select a backward Euler dynamic timestepping scheme. Define

$$\begin{aligned} 0 &= t_0 < t_1 < \dots \\ \vec{U}^n &= \vec{U}(t_n) \end{aligned} \quad n \in \mathbb{Z}_0^+$$

so

$$\begin{aligned} 0 &= M \frac{\vec{U}^n - \vec{U}^{n-1}}{\Delta t_n} + S \vec{U}^n \\ 0 &= M (\vec{U}^n - \vec{U}^{n-1}) + \Delta t_n S \vec{U}^n \\ 0 &= (M + \Delta t_n S) \vec{U}^n - M \vec{U}^{n-1} \end{aligned}$$

yielding the matrix equation

$$(M + \Delta t_n S) \vec{U}^n = M \vec{U}^{n-1}$$

Due to accuracy needing small h_p , Simpson's Rule with two subintervals is used to evaluate the integral for the mass matrix to avoid machine rounding errors via division by small h_p values.

$$\int_a^b f(x) dx \approx \frac{b-a}{6} \left[f(a) + 4f\left(\frac{a+b}{2}\right) + f(b) \right]$$

Additionally, note the diagonalism, i.e.

$$\begin{aligned} [M]_{pq} &= [M]_{qp} \\ [S]_{pq} &= [S]_{qp} \end{aligned}$$

thus, WLOG we calculate

$$\begin{array}{lll} [M]_{pp}, [S]_{pp} & p \in \mathbb{P} & \text{(diagonal)} \\ [M]_{p-1,p}, [S]_{p-1,p} & p \in \mathbb{P}^+ & \text{(off-diagonal)} \end{array}$$

For clarity, define

$$\begin{aligned} \mathbb{P}_- &= \{0, \dots, P-1\} \\ \mathbb{P}_+ &= \{1, \dots, P\} \\ R'(s) &= R(s) \sin(\omega(s)) \\ D'(s) &= D(s) \sin(\omega(s)) \end{aligned}$$

9.4 Mass Matrix

For the main diagonal,

$$\begin{aligned} [M]_{pp} &= \langle \Lambda_p^2(s) \rangle \\ &= \int_{\Gamma} R'(s) \Lambda_p^2(s) ds \\ &= I_{\mathbb{P}_+}(p) \int_{s_{p-1}}^{s_p} R'(s) \frac{s - s_{p-1}}{h_p} ds + I_{\mathbb{P}_-}(p) \int_{s_p}^{s_{p+1}} R'(s) \frac{s_{p+1} - s}{h_{p+1}} ds \end{aligned}$$

where the first integral is

$$\begin{aligned} &\int_{s_{p-1}}^{s_p} R'(s) \frac{s - s_{p-1}}{h_p} ds \\ &= \frac{1}{h_p} \int_{s_{p-1}}^{s_p} R'(s)(s - s_{p-1}) ds \\ &\approx \frac{1}{6} \left[R'(s_p)h_p + 4R'(s_{p-1/2}) \left(\frac{s_{p-1} + s_p}{2} - s_{p-1} \right) \right] \\ &= \frac{1}{6} [R'(s_p)h_p + 2R'(s_{p-1/2})h_p] \end{aligned}$$

and the second integral is

$$\begin{aligned}
& \int_{s_p}^{s_{p+1}} R'(s) \frac{s_{p+1} - s}{h_{p+1}} ds \\
&= \frac{1}{h_p} \int_{s_p}^{s_{p+1}} R'(s)(s_{p+1} - s) ds \\
&\approx \frac{1}{6} \left[R'(s_p)h_{p+1} + 4R'(s_{p+1/2}) \left(s_{p+1} - \frac{s_p + s_{p+1}}{2} \right) \right] \\
&= \frac{1}{6} [R'(s_p)h_{p+1} + 2R'(s_{p+1/2})h_{p+1}]
\end{aligned}$$

so

$$[M]_{pp} \approx \frac{1}{6} (I_{\mathbb{P}_+}(p)h_p[R'(s_p) + 2R'(s_{p-1/2})] + I_{\mathbb{P}_-}(p)h_{p+1}[R'(s_p) + 2R'(s_{p+1/2})])$$

For the off-diagonals,

$$\begin{aligned}
[M]_{p-1,p} &= \langle \Lambda_{p-1}(s) \Lambda_p(s) \rangle \\
&= \int_{\Gamma} R'(s) \Lambda_{p-1}(s) \Lambda_p(s) ds \\
&= \frac{1}{h_p^2} \int_{s_{p-1}}^{s_p} R'(s)(s_p - s)(s - s_{p-1}) ds \\
&\approx \frac{1}{6h_p} \left[4R'(s_{p-1/2}) \left(s_p - \frac{s_{p-1} + s_p}{2} \right) \left(\frac{s_{p-1} + s_p}{2} - s_{p-1} \right) \right]
\end{aligned}$$

yielding

$$[M]_{p-1,p} \approx \frac{h_p}{6} R'(s_{p-1/2})$$

9.5 Stiffness Matrix

For the main diagonal,

$$\begin{aligned}
[S]_{pp} &= \left\langle \frac{D(s)}{R(s)} \left(\frac{\partial \Lambda_p(s)}{\partial s} \right)^2 \right\rangle \\
&= \int_{\Gamma} D'(s) \left(\frac{\partial \Lambda_p(s)}{\partial s} \right)^2 ds \\
&= I_{\mathbb{P}_+}(p) \int_{s_{p-1}}^{s_p} D'(s) \frac{1}{h_p^2} ds + I_{\mathbb{P}_-}(p) \int_{s_p}^{s_{p+1}} D'(s) \frac{1}{h_{p+1}^2} ds \\
&= \frac{I_{\mathbb{P}_+}(p)}{h_p^2} \int_{s_{p-1}}^{s_p} D'(s) ds + \frac{I_{\mathbb{P}_-}(p)}{h_{p+1}^2} \int_{s_p}^{s_{p+1}} D'(s) ds
\end{aligned}$$

and the off diagonals,

$$\begin{aligned}
[S]_{p-1,p} &= \left\langle \frac{D(s)}{R(s)} \frac{\partial \Lambda_{p-1}(s)}{\partial s} \frac{\partial \Lambda_p(s)}{\partial s} \right\rangle \\
&= \int_{\Gamma} D'(s) \frac{\partial \Lambda_{p-1}(s)}{\partial s} \frac{\partial \Lambda_p(s)}{\partial s} \, ds \\
&= \int_{s_{p-1}}^{s_p} D'(s) \frac{-1}{h_p^2} \, ds \\
&= \frac{-1}{h_p^2} \int_{s_{p-1}}^{s_p} D'(s) \, ds
\end{aligned}$$

Chapter 10

TIRF Microscopy Model

The final component of the intended model is incorporation of parameters involved in TIRF Microscopy which limit the resolution of observations for fusion and diffusion dynamics in space and time.

10.1 TIRF Microscopy Zone

By nature of the evanescent wave, observations are limited to a depth below the viewing platform. Let this depth be denoted $d_m > 0$. The viewing angle for full and kiss-and-run fusion is thus

$$\begin{aligned}\varphi_m &= \min \left\{ \pi, \arccos \left(1 - \frac{d_m}{R'} \right) \right\} \\ \phi_m &= \max \left\{ \pi, \arccos \left(1 - \frac{d_m}{R'_v} \right) \right\} \\ \psi_m &= \min \left\{ \pi, \arccos \left(1 - \frac{d_m}{R'_c} \right) \right\}\end{aligned}$$

10.2 Spot Intensity

10.3 Ring Intensity

Part III

Implementation

Chapter 11

Application Programming Interface

11.1 Fusion Modes

11.2 Diffusion

11.3 Intensity

11.3.1 Point Spread Function

11.3.2 TIRF Zone

11.3.3 Spot Intensity

11.3.4 Ring Intensity

Chapter 12

Tests

For each run of the diffusion model, there are a number of tests that can be performed on the resulting solution.

12.1 Total Concentration

By the law of mass conservation, the integrated concentration $\langle u \rangle$ must be constant. This is easy to check.

12.2 Junction Flux

For all timesteps, it is expected that the solution satisfy the junction flux relationship specified by TODO.

12.3 Steady State

This test is actually incorporated as the stopping condition for the solving loop. Once the solution is proven to be converging uniformly to the steady state value within a tolerance, the loop ends.

Chapter 13

Model Usage

Due to the diminutive nature of cells and vesicles, the model implementation would require a very small stepping size. Fortunately, the units used in the model only require consistency, thus input units are specified when used.

Part IV

Mode Discernment

Chapter 14

Total Concentration on Fused Vesicle Membrane

One metric for mode discernment in the theoretical space is the rate of decrease of total concentration on the vesicle.

Chapter 15

TIRF Microscopy Simulation

Chapter 16

Regional Intensity

16.1 Spot Intensity

16.2 Ring Intensity

16.3 Point Spread

16.4 TIRF Zone

16.5 Frame Rate

Chapter 17

Discernment

17.1 General Conclusions

17.2 Applications

17.2.1 Beta Cells

[Marchetti et al., 2017] reported an average β cell radius of $R_c = 10 \mu\text{m}$.

Bibliography

- [Marchetti et al., 2017] Marchetti, P., Bugliani, M., De Tata, V., Suleiman, M., and Marselli, L. (2017). Pancreatic beta cell identity in humans and the role of type 2 diabetes. *Frontiers in cell and developmental biology*, 5:55.
- [Milo et al., 2010] Milo, R., Jorgensen, P., Moran, U., Weber, G., and Springer, M. (2010). Bionumbers—the database of key numbers in molecular and cell biology. *Nucleic acids research*, 38(suppl_1):D750–D753.
- [Soult et al., 2020] Soult, A., Bewick, S., Parsons, R., Forsythe, T., Robinson, S., and Dupon, J. (2020). *Phospholipids in cell membranes*. LibreTexts.